© 2018. Published by The Company of Biologists Ltd | Development (2018) 145, dev167023. doi:10.1242/dev.167023

RESEARCH ARTICLE

The Hippo pathway effector Taz is required for cell morphogenesis and fertilization in zebrafish

Chaitanya Dingare[1,2], Alina Niedzwetzki[1], Petra A. Klemmt[1], Svenja Godbersen[2], Ricardo Fuentes[3], Mary C. Mullins[3] and Virginie Lecaudey[1,2,*]

ABSTRACT

Hippo signaling is a critical pathway that integrates extrinsic and intrinsic mechanical cues to regulate organ size. Despite its essential role in organogenesis, little is known about its role in cell fate specification and differentiation. Here, we unravel a novel and unexpected role of the Hippo pathway effector Taz (*wwtr1*) in controlling the size, shape and fate of a unique cell in the zebrafish ovary. We show that *wwtr1* mutant females are infertile. In teleosts, fertilization occurs through the micropyle, a funnel-like opening in the chorion, formed by a unique enlarged follicle cell, the micropylar cell (MC). We describe here, for the first time, the mechanism that underlies the differentiation of the MC. Our genetic analyses show that Taz is essential for MC fate acquisition and subsequent micropyle formation in zebrafish. We identify Taz as the first bona fide MC marker and show that Taz is specifically and strongly enriched in the MC precursor. Altogether, we performed the first genetic and molecular characterization of the MC and propose that Taz is a key regulator of MC fate.

This article has an associated 'The people behind the papers' interview.

KEY WORDS: Taz, Hippo, Fertilization, Micropyle, Micropylar cell, Zebrafish

INTRODUCTION

Developmental biologists have been interested in the molecular and cellular mechanisms driving cell fate specification and cell differentiation over the last few decades. Acquisition of a specific cell fate results from a combination of biochemical and physical cues, but how cells interpret these cues in a combinatorial manner to adopt a fate different from their neighbors is still unclear. To address this issue, we have used the zebrafish ovarian follicle epithelium as a model.

Fertilization is a key event in the life cycle of all sexually reproducing organisms, but is achieved differently in different species. In teleosts, a sperm penetrates the oocyte through a narrow canal called the 'micropyle' that traverses the thick vitelline membrane. The micropyle is formed by a specialized follicle cell, the micropylar cell (MC), that differentiates during oogenesis and around which vitelline material is deposited (Hart and Donovan, 1983; Kobayashi and Yamamoto, 1985; Nakashima and Iwamatsu, 1989; Selman et al., 1993).

Oogenesis in zebrafish can be divided into five stages (Selman et al., 1993) (Fig. 1A). During stage I, individual oocytes become surrounded by follicle cells (FCs) and components of the vitelline membrane begin to accumulate in between. At this stage, the Balbiani body forms at the future vegetal pole and determines the oocyte animal-vegetal (AV) axis (Marlow and Mullins, 2008). During Stage II, both FCs and the oocyte extend microvilli that contact each other via cell-cell junctions. During stage III, the MC becomes morphologically distinguishable from other FCs. During stage IV, the germinal vesicle migrates to the animal pole and the oocyte and FCs retract their microvilli prior to ovulation. Finally, during stage V, the mature egg, free of FCs, is released, and can be fertilized by the sperm through the micropyle (Selman et al., 1993).

How can a modified FC perforate the vitelline membrane? Electron microscopy (EM) analyses in Medaka and the Chum salmon have provided the first insights into how the MC morphology determines the micropyle architecture (Kobayashi and Yamamoto, 1985; Nakashima and Iwamatsu, 1989). In these species, the MC enlarges compared with other FCs and adopts a stereotypical mushroom-shape. The proximal part of the 'mushroom' (closest to the oocyte) forms a cytoplasmic extension, which contains intertwined bundles of microtubules and tonofilaments, and remains in contact with the oocyte cell surface, also known as the oolemma. The cytoplasmic extension is thought to either prevent accumulation of vitelline material and/or to apply mechanical pressure on the growing vitelline membrane. Finally, the MC shrinks at the end of oogenesis and withdraws from the micropylar canal, leaving a hole in the vitelline membrane (Fig. 1A, Stage V) (Kobayashi and Yamamoto, 1985; Nakashima and Iwamatsu, 1989). Despite this detailed ultra-structural description, no molecular marker for the MC has been identified so far. Furthermore, almost nothing is known about the genetic and molecular mechanisms that lead to the specification and differentiation of the MC.

The MC invariably forms at the animal pole of the oocyte. In zebrafish *bucky ball* (*buc*) mutant oocytes, the Balbiani body fails to form and the oocyte displays a radially expanded animal pole identity and lacks the vegetal pole (Bontems et al., 2009; Marlow and Mullins, 2008). As a result, multiple micropyles form around the oocyte, leading to polyspermy (Marlow and Mullins, 2008). This demonstrates the importance of oocyte polarity establishment to spatially restrict the MC. This and subsequent studies suggest that the wild-type (WT) oocyte signals to the FC layer to position and induce the specification of the MC at the animal pole only (Heim et al., 2014). However, the mechanisms that underlie the selection and the differentiation of the MC remain completely unknown.

The Hippo signaling pathway was discovered less than 15 years ago in *Drosophila* and subsequently shown to be conserved in vertebrates (Huang et al., 2005; Zhao et al., 2007, reviewed by Dong

[1]Institute of Cell Biology and Neuroscience, Department of Developmental Biology of Vertebrates, Goethe Universität Frankfurt am Main, Max-von-Laue-Straße 13, 60438 Frankfurt am Main, Germany. [2]Developmental Biology, Institute for Biology I, Faculty of Biology, Albert-Ludwigs-Universität Freiburg, 79104 Freiburg, Germany. [3]University of Pennsylvania Perelman School of Medicine, Department of Cell and Developmental Biology, 421 Curie Blvd., Philadelphia, PA 19104, USA.

*Author for correspondence (lecaudey@bio.uni-frankfurt.de)

C.D., 0000-0002-5116-4721; M.C.M., 0000-0002-9979-1564; V.L., 0000-0002-8713-3425

Received 11 May 2018; Accepted 9 October 2018

Development (2018) 145, dev167023. doi:10.1242/dev.167023

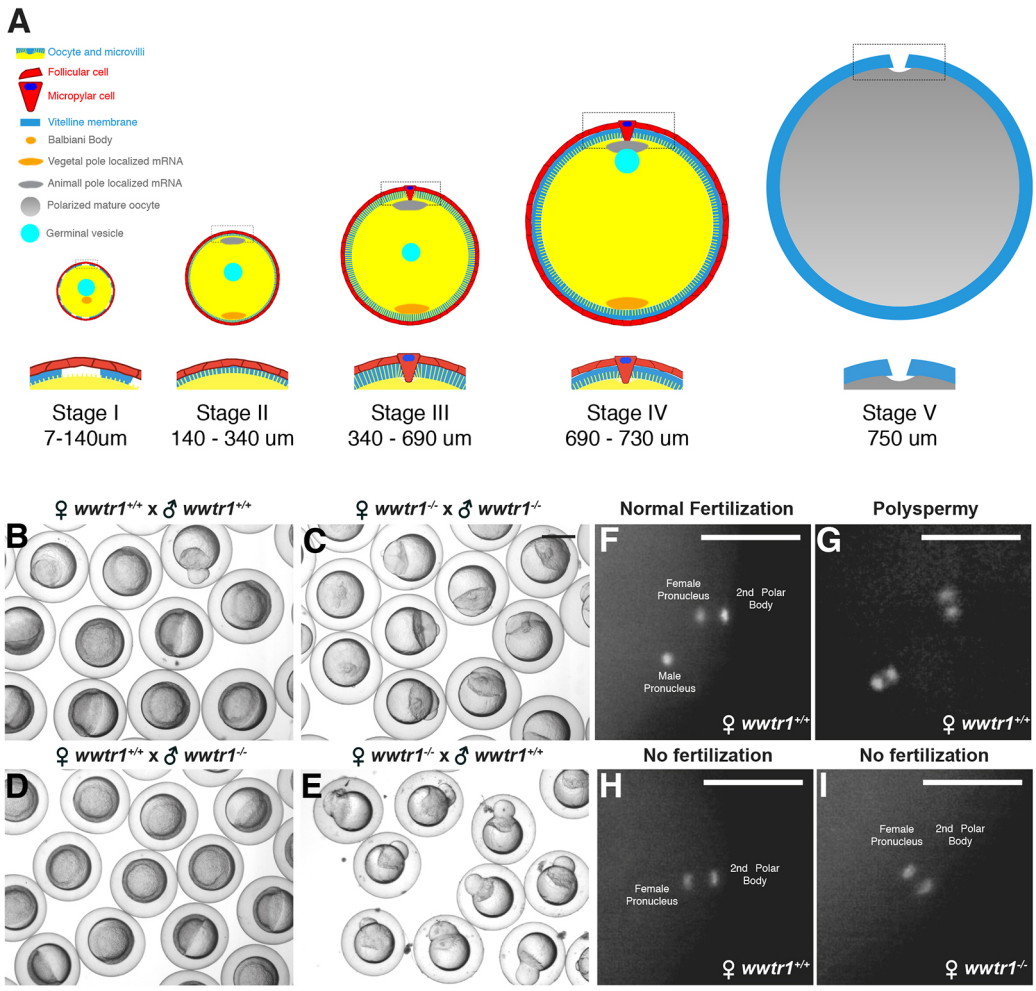

Fig. 1. *wwtr1* mutant females are infertile. (A) Scheme representing the five different stages of zebrafish oogenesis. (B-E) Eggs or shield stage embryos from a *wwtr1*$^{+/+}$ incross (B, *N*=3), a *wwtr1*$^{-/-}$ incross (C, *N*=3), an outcross of *wwtr1*$^{-/-}$ males to WT females (D, *N*=3) or an outcross of *wwtr1*$^{-/-}$ females to WT males (E, *N*=3) (Table S1). (F-I) Eggs from *wwtr1*$^{+/+}$ (F-H, *N*=2, *n*=40) or *wwtr1*$^{-/-}$ females (I, *N*=2, *n*=40) fertilized *in vitro* with WT sperm and stained with DAPI. *N*, number of experiments; *n,* number of samples. Scale bars: 50 µm in F-I.

et al., 2007; Pan, 2007). In vertebrates, the core Hippo kinase cascade leads to the phosphorylation of the two transcriptional effectors yes-associated protein (YAP) and transcriptional co-activator with PDZ-binding motif (TAZ) and to their sequestration and/or degradation in the cytoplasm. In contrast, when the core kinase cascade is inactive, YAP and TAZ can translocate into the nucleus and act as co-factors of transcription to activate the expression of genes that promote cell proliferation, growth or survival. This core Hippo kinase cascade is also referred to as the 'canonical' Hippo pathway.

Recently, several proteins that are associated with cell junctions or apico-basal polarity have been proposed to limit YAP and TAZ function independently of the core kinase cascade, thus constituting the 'non-canonical' Hippo pathway (reviewed by Varelas, 2014; Zhao et al., 2011). In addition to their role in limiting organ size, YAP and TAZ are involved in other cellular processes, including cell fate specification (Beyer et al., 2013; Judson et al., 2012; Miesfeld et al., 2015; Musah et al., 2014; Yimlamai et al., 2014; Zhang et al., 2011). YAP is, for example, essential for the specification of trophectoderm versus inner cell mass in the mammalian blastocyst downstream of both cell polarity and cell adhesion (reviewed by Hirate et al., 2013; Leung and Zernicka-Goetz, 2013; Nishioka et al., 2009).

Here, we investigate the role of the Hippo pathway effector Taz, encoded by the *WW domain-containing transcription regulator protein 1* gene (*wwtr1*), in zebrafish oogenesis. We show that *wwtr1/taz* mutant females lay eggs that cannot be fertilized because they lack a micropyle. While oogenesis progressed normally in the mutant females, we found that the MC failed to differentiate. We show that Taz is strongly enriched in the future MC before morphological changes, making Taz the first bona fide marker of this somatic cell type. By using markers for cell junctions and the cytoskeleton, we characterized the MC at the molecular level for the first time. Our results indicate that Taz is required very early for the transition from an FC to an MC, either for specification of the MC or for its early differentiation. These results open the door for further gene function discovery in micropyle biogenesis. We propose a working model that links oocyte polarity, Taz function and MC fate determination and differentiation.

RESULTS

wwtr1 mutant females are infertile

To address the function of Taz during embryonic development, we generated a TALEN mutant. We recovered several alleles including *wwtr1*^{fu55} (hereafter called *wwtr1*$^{-}$). The induced genomic lesion in the first exon creates a premature stop codon after 29 amino acids

Development (2018) 145, dev167023. doi:10.1242/dev.167023

(Fig. S1A-C). The zygotic mutant embryos did not show any obvious morphological phenotype and grew to adults that were indistinguishable from their siblings (Fig. S1D,E). In contrast, when these homozygous mutant adults were incrossed, all eggs failed to undergo cleavage and appeared as unfertilized eggs (Fig. 1C), whereas eggs from WT sibling (Fig. 1B) or heterozygote incrosses (Table S1) developed normally.

To further test whether this phenotype was maternal or paternal, *wwtr1*$^{-/-}$ mutants were outcrossed to WT. Whereas eggs from crosses between *wwtr1*$^{-/-}$ males and WT females underwent cleavage normally (Fig. 1D), eggs from crosses between *wwtr1*$^{-/-}$ females and WT males did not undergo cleavage (Fig. 1E). To ensure that the observed phenotype was due to the loss of Taz function, we performed a complementation experiment by combining in trans our *wwtr1*^{fu55} allele and the previously published *wwtr1*^{mw49} allele (Miesfeld et al., 2015). Whereas eggs from *wwtr1*$^{mw49/+}$ females crossed with WT males developed normally (Fig. S1F-H), none of the eggs laid by *wwtr1*$^{mw49/fu55}$ females underwent cleavage (Fig. S1I-K). Altogether, these results suggest that the maternal absence of Taz affects the competence of the eggs to be fertilized.

To test this possibility, we performed *in vitro* fertilization (IVF) assays with eggs from *wwtr1*$^{-/-}$ and *wwtr1*$^{+/+}$ females with WT sperm. Eggs were fixed after 10 min and stained with DAPI. In most of the control eggs, three DAPI-positive dots could be identified, corresponding to the male and female pronucleus and DNA of the 2nd polar body (Fig. 1F, 24/40). Occasionally, four (4/40) or two (12/40) DAPI-positive dots were observed, corresponding to either polyspermy events, which are often reported in IVF assays (Fig. 1G), or to unfertilized eggs (Fig. 1H), respectively. In contrast, in all eggs obtained from *wwtr1*$^{-/-}$ females (40/40), only two nuclei were detected, corresponding to the female pro-nucleus and the 2nd polar body DNA (Fig. 1I), identical to unfertilized eggs (compare with Fig. 1H). This result indicates that eggs laid by *wwtr1*$^{-/-}$ females cannot be fertilized.

wwtr1 mutant eggs lack a functional micropyle

To determine the cause of this infertility, we dissected out ovaries from *wwtr1*$^{-/-}$ and *wwtr1*$^{+/-}$ females. The overall morphology of *wwtr1*$^{+/-}$ (Fig. S2A) and *wwtr1*$^{-/-}$ (Fig. S2B) ovaries was indistinguishable, which suggests that the infertility was not caused by defective oogenesis. To test whether the micropyle formed properly, mature eggs from *wwtr1*$^{+/-}$ and *wwtr1*$^{-/-}$ females were extruded, activated in E3 and the micropyle was observed after staining with Coomassie Brilliant Blue (CBB), which binds to glycoproteins that are enriched in the micropylar structure (Yanagimachi et al., 2013). Whereas the micropyle could be easily identified on the expanded chorion of eggs obtained from *wwtr1*$^{+/-}$ females (arrow in Fig. 2A,A′, see also Fig. S2C,C′), such a structure was never observed in eggs obtained from *wwtr1*$^{-/-}$ females (Fig. 2B,B′,D,D′). These data indicate that the micropyle fail to form in females lacking Taz activity.

To determine whether the absence of the micropyle was the sole cause of infertility in *wwtr1*$^{-/-}$ females, we attempted to bypass the barrier of the chorion. Since intracytoplasmic sperm injection is not possible because it requires a micropyle to inject sperm through (Poleo et al., 2001), we enzymatically removed the chorion before the IVF. With this procedure, the fertilization rate of eggs obtained from *wwtr1*$^{+/-}$ (n=685) and from *wwtr1*$^{-/-}$ (n=649) females was identical and equal to 24% (Fig. 2C-E and Table S2). These results demonstrate that the eggs from *wwtr1*$^{-/-}$ females have the capacity to be fertilized and develop further if the barrier of the chorion is eliminated. Therefore the sole cause of infertility in females lacking Taz activity is the absence of the micropyle.

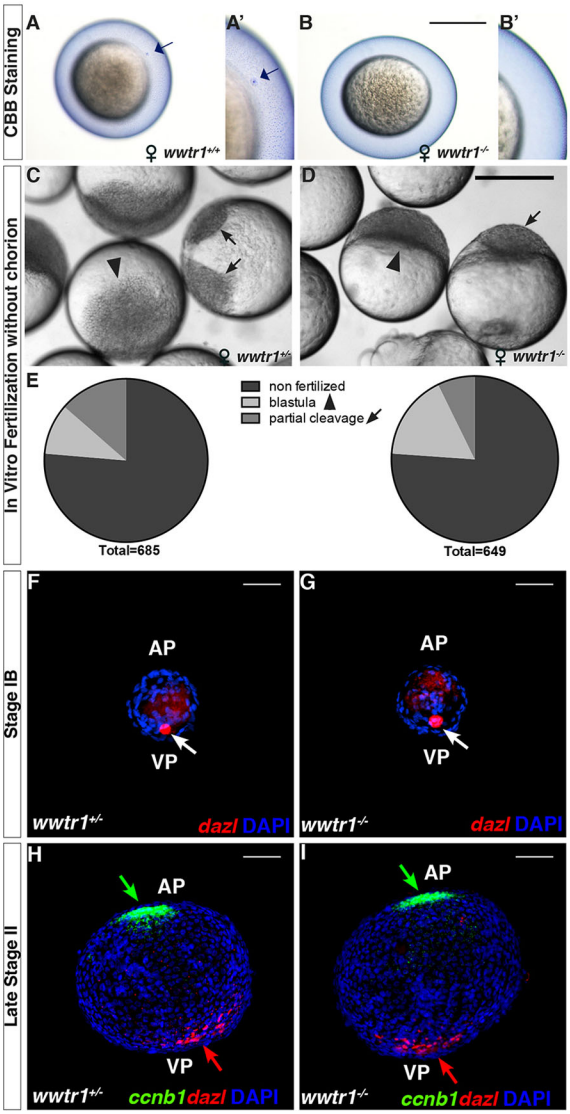

Fig. 2. Eggs from *wwtr1*$^{-/-}$ females do not form a micropyle. (A-B′) The micropyle is stained by Coomassie Brilliant Blue in activated eggs from *wwtr1*$^{+/+}$ females (A,A′, n=10) but not from *wwtr1*$^{-/-}$ females (B,B′, n=8). Arrows indicate the micropyle. (C-E) Blastula (arrowhead) or partially cleaved (black arrows) eggs from *wwtr1*$^{+/-}$ (C) or *wwtr1*$^{-/-}$ (D) females fertilized *in vitro* after enzymatic removal of the chorion and corresponding quantification (E). (F-I) WISH with the Balbiani body marker *dazl* (F-I, red arrow) and the animal pole marker *ccnb1* (H,I, green arrow) in *wwtr1*$^{+/-}$ (F,H, n=39) and *wwtr1*$^{-/-}$ (G, I, n=31) oocytes at the indicated stage of oogenesis. FC nuclei are stained with DAPI. AP, animal pole; VP, vegetal pole. Scale bars: 50 µm in F-I; 500 µm in A-D.

wwtr1 mutant oocytes exhibit normal animal-vegetal polarity

In the zebrafish *buc* mutant, in which AV polarity fails to be established, supernumerary micropyles form due to radial animal identity, leading to polyspermy (Marlow and Mullins, 2008). To test whether the absence of a micropyle in eggs from *wwtr1*$^{-/-}$ females could be because of a loss of animal pole identity, we investigated AV polarity formation in *wwtr1*$^{-/-}$ oocytes. The *dazl* mRNA, one of the first transcripts to localize asymmetrically, localizes to the Balbiani Body as early as stage IB of oogenesis and then at the

Development (2018) 145, dev167023. doi:10.1242/dev.167023

vegetal pole of the oocyte (Elkouby et al., 2016; Maegawa et al., 1999). The *cyclin B1* (*ccnb1*) mRNA localizes at the animal pole from late stage II of oogenesis onward (Howley and Ho, 2000). In oocytes from both *wwtr1*$^{-/-}$ and *wwtr1*$^{+/-}$ females, the *dazl* and *ccnb1* mRNA localized at opposite poles (Fig. 2F-I). This indicates that the Balbiani body forms properly in *wwtr1*$^{-/-}$ oocytes, the absence of the micropyle in eggs from *wwtr1*$^{-/-}$ females is not due to a disruption of oocyte AV polarity and, conversely, the absence of the micropyle does not seem to affect oocyte polarity.

The micropylar cell fails to differentiate in the absence of Taz activity

Since the micropyle is formed by the MC, which differentiates at the animal pole, we further tested whether the loss of the micropyle in eggs from *wwtr1*$^{-/-}$ females is due to defective MC formation. For this purpose, we first analysed the organization of the follicle cell layer (FCL) at the animal pole by combining whole-mount *in situ* hybridization (WISH) to the animal pole marker *ccnb1* with DAPI to label the FC nuclei. At late stage II of oogenesis, the FCL was homogeneously organized at the animal pole both in *wwtr1*$^{+/+}$ (Fig. 3A-D) and in *wwtr1*$^{-/-}$ follicles (Fig. 3I-L). In the stage III oocyte, control FCs at the animal pole assumed a typical concentric arrangement around the centrally located MC (Fig. 3E-H, green arrow). In contrast, *wwtr1*$^{-/-}$ FCs showed a disorganized animal pole arrangement at this stage and no MC could be identified (Fig. 3M-P). In addition, an indentation was often present (51% of the cases) in the center of the *ccnb1*-positive domain in which the MC would usually form (Fig. 3P, red arrow). Intriguingly, the indentation was significantly deeper in *wwtr1*$^{-/-}$ compared with *wwtr1*$^{+/+}$ oocytes (Fig. 3P-R and Fig. S3E-G).

To determine whether the MC is present but fails to differentiate, or whether it is completely absent in *wwtr1*$^{-/-}$ mutants, we labeled late stage III follicles with Rhodamine Phalloidin to delineate cell morphology, along with the *zp0.5:egfp-zorba* transgene to mark the animal pole (Fig. S3A-D. See the Materials and Methods section). The large MC was sharply delineated in *wwtr1*$^{+/-}$ follicles, stretching from the FCL to the oocyte surface (green arrow in Fig. 3Q; yellow bracket in Fig. 3Q-R marks the FCL) and surrounded by microvilli. In contrast, no distinct cell was present at the animal pole in the FCL of *wwtr1*$^{-/-}$ follicles (Fig. 3R). Instead a gap that was neither filled by a cell nor by microvilli was present between the FCL and the oocyte surface (green bracket in Fig. 3R). As shown above in Fig. 3P, an indentation was present in the oolemma despite the absence of a differentiated MC (red arrow, Fig. 3R). This suggests that, in the absence of the MC, the FCL does not adhere to the oocyte surface at the level of the animal pole. Altogether, these results show that, in the absence of Taz activity, the MC fails to form, indicating that Taz is required either very early for the differentiation of the MC or for its specification.

Taz is the first bona fide marker of the micropylar cell

To understand how Taz acts in MC formation, we investigated whether Taz is expressed in the oocyte or in the FCs. RT-PCR on non-activated eggs and embryos before and after the maternal-zygotic transition indicate that *wwtr1* mRNA was not present before 60% epiboly (Fig. S4A). *wwtr1* mRNA is therefore not maternally provided, which suggests that it may be expressed in the FCL. To test this hypothesis, we stained stage III oocytes with an anti-Taz antibody, combined with β-catenin and DAPI staining to label cell membranes and nuclei, respectively. Strikingly, Taz protein appeared highly enriched in one cell at the surface of the FC layer (Fig. 4A). This cell was easily identifiable as the MC based on the regular organization of the other FC nuclei around it (Fig. 4B). β-Catenin was specifically weaker at the lateral membrane of the MC compared with surrounding FCs (Fig. 4C,D). Orthogonal sections also showed that the Taz-positive cell is much bigger than other FCs and has the typical mushroom-like morphology (Fig. 4E), confirming that this is the MC. Accordingly, Taz was also highly enriched in the ectopic MCs specified in the *buc* mutant (Fig. 4F-G′). Altogether, these data identify Taz as the first bona fide marker of the MC.

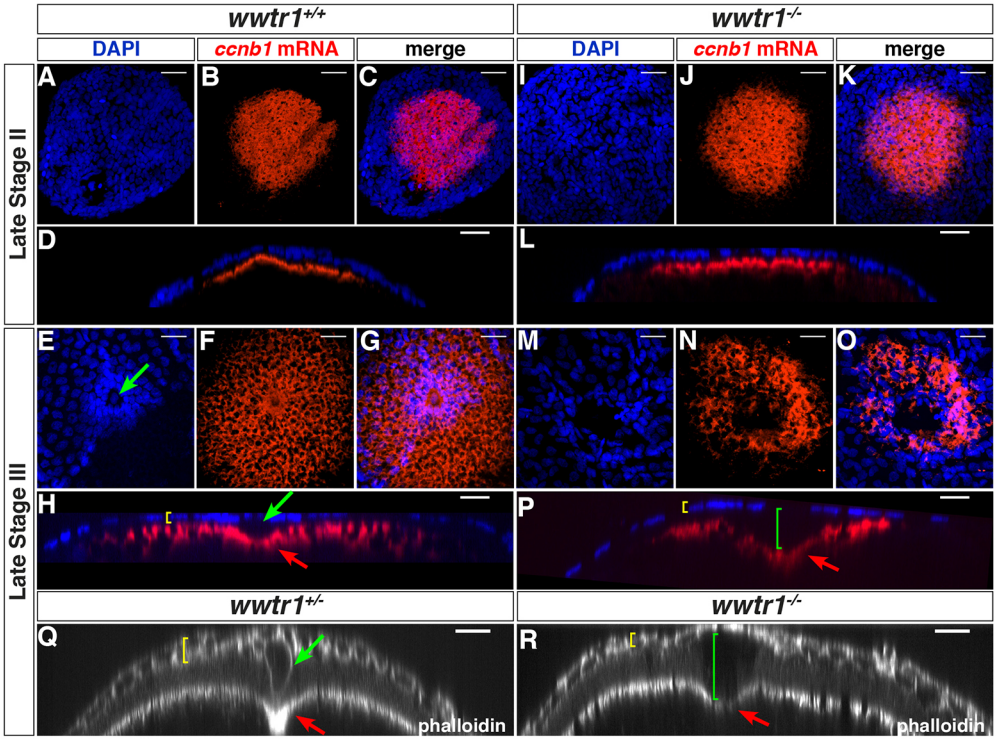

Fig. 3. *wwtr1* mutant follicles lack the micropylar cell. (A-P) Maximum intensity projection of confocal images of *wwtr1*$^{+/+}$ (A-H, *n*=31) or *wwtr1*$^{-/-}$ (I-P, *n*=40) follicles stained by ISH to detect *ccnb1* mRNA at the animal pole (red), combined with DAPI nuclear staining (blue) at the indicated oocyte stages. (D,L,H,P) Orthogonal views of corresponding confocal stacks (C,K,G, O). (Q-R) Orthogonal views of confocal stacks of *wwtr1*$^{+/-}$ (Q, *n*=9) or *wwtr1*$^{-/-}$ (R, *n*=7) follicles stained with Rhodamine Phalloidin. Green arrows indicate an MC; red arrows indicate the indentation of the oolemma; yellow brackets indicate the FCL; green brackets indicate the gap between the FCL and the oocyte surface in *wwtr1*$^{-/-}$ follicles. The *zp0.5:egfp-zorba* transgene (not shown) was used to localize the animal pole and orient the follicles. Scale bars: 20 µm.

Development (2018) 145, dev167023. doi:10.1242/dev.167023

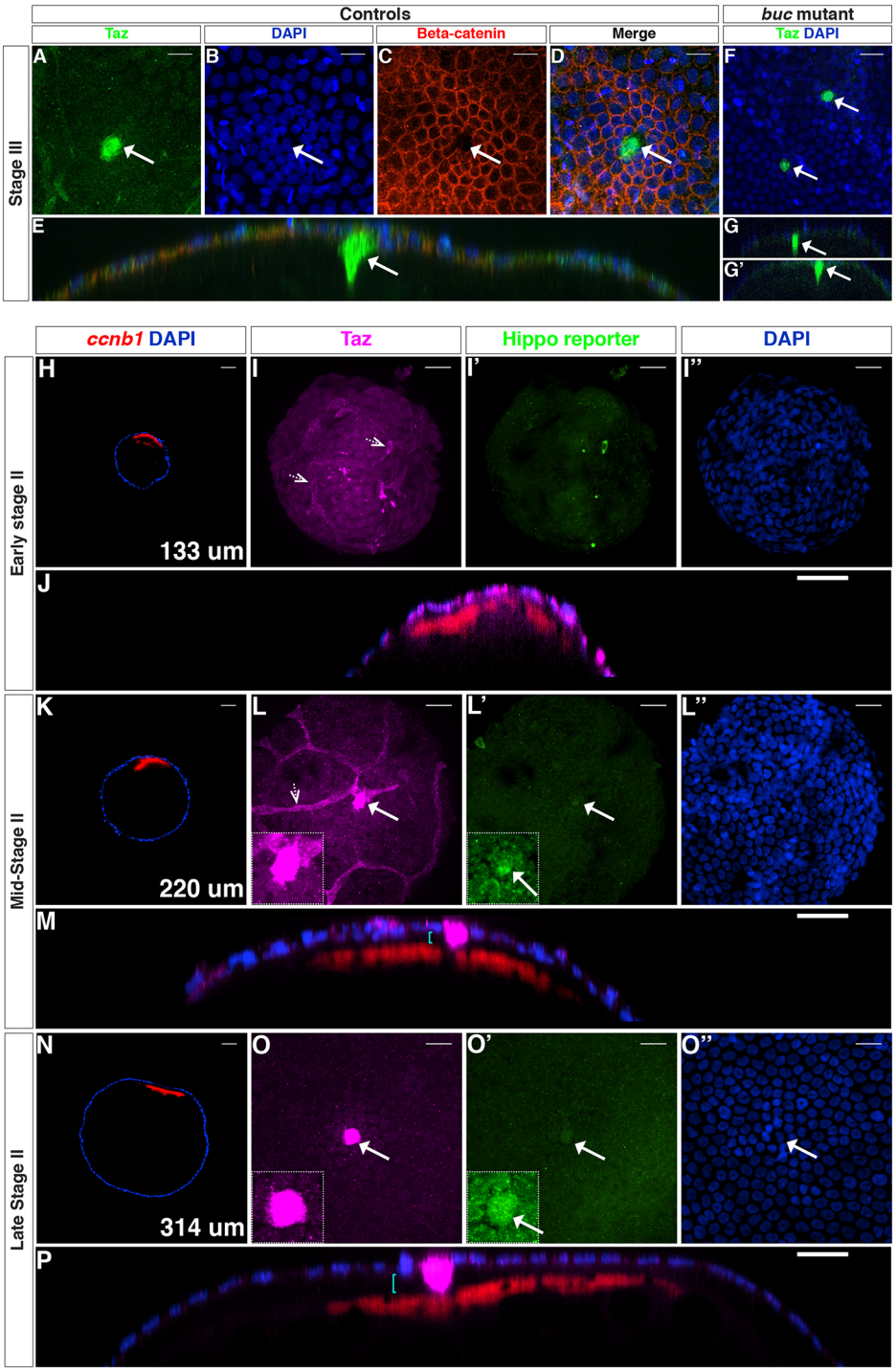

Fig. 4. Taz protein is a bona fide marker of the MC. (A-E) Confocal images of stage III WT oocytes stained with anti-Taz (A) and anti-β-catenin (C) antibodies, and DAPI (B, *n*=4). D shows the three channels merged, and E is an orthogonal view of D. (F-G′) Stage III *buc* mutant oocytes stained with the anti-Taz antibody and DAPI (*n*=4). G and G′ are orthogonal views of F. (H-P) Confocal images of wholemount *Tg(4xGTIIC:d2egfp)*$^{mw50/0}$ oocytes stained with the anti-Taz antibody (magenta), *ccnb1* mRNA (red) and DAPI (blue) at early stage II (H-J), mid-stage II (K-M) and late stage II (N-P) (*n*=38). Hippo reporter activity is shown in green. Cyan brackets in orthogonal views (M,P) indicate the gap between the oocyte surface and the FC layer (microvilli are not visible); white arrows indicate an MC; dotted arrowheads (I,L) point to non-follicle cells. Insets in L,L′,O,O′ show higher magnification of center of panel. Scale bars: 20 µm in A-D,F,I,J, L,M,O,P; 40 µm in H,K,N.

To gain more insights into the role of Taz in the formation of the MC, we determined how early Taz protein is enriched in the MC, using *ccnb1* mRNA localization to mark the animal pole. In addition, to evaluate Taz activity, follicles were dissected from Tg(*4xGTIIC:d2egfp*)^{mw50} females that expressed the Hippo/TEA domain transcription factors (TEAD) reporter or were stained with an antibody against connective tissue growth factor (CTGF), a bona fide YAP/TAZ target (Miesfeld and Link, 2014; Zhao et al., 2008). In early stage II oocytes (Fig. 4H, follicle size 133 µm), Taz protein levels and the GFP signal from the TEAD reporter line were homogenous and very low in the entire FC layer (Fig. 4I-J). From mid-stage II onwards (Fig. 4K, follicle size 220 µm), the levels of Taz protein and of the TEAD reporter increased in the MC precursor compared with the rest of the FCs (Fig. 4L-M, arrow). In late stage II oocytes (Fig. 4N, follicle size 314 µm), Taz levels were very high in the MC and the TEAD reporter activity was also elevated compared with the other FCs (Fig. 4O-P, arrows). Accordingly, CTGF was enriched in one single cell at the animal pole of the FCL in *wwtr1*$^{+/-}$ follicles (Fig. S4B-C′′), but was absent in stage-matched *wwtr1*$^{-/-}$ follicles (Fig. S4D-E′′). These results show that Taz is enriched and active in the MC precursor from mid-stage II onward. This suggests that Taz could be one of the very first factors required for the specification and/or differentiation of the MC.

Development (2018) 145, dev167023. doi:10.1242/dev.167023

Tight and adherens junctions mediate the contact between the MC and the oocyte

To better understand the transition from FC to MC and the role of Taz in this process, we further characterized the MC and its contact with the oocyte at the molecular level. First, we examined tight junctions (TJs), which have been proposed to be present at the contact point between the oocyte and the MC in other species (Kobayashi and Yamamoto, 1985). We combined an antibody against Zonula occludens-1 (ZO-1; also known as Tjp1a) with the *egfp-zorba* transgene to localize the animal pole (not shown). In control oocytes at early stage III, a thick actin accumulation (solid arrow in Fig. S5A) was observed in the cortical actin layer immediately beneath the MC-oocyte contact point and a weak ZO-1 staining was detected in the center of the actin-rich zone (simple arrow Fig. S5A′-B′). In mid-stage III oocytes, the thick actin accumulation persisted (solid arrows in Fig. S5C) and ZO-1 appeared as a thin ring, included within the thicker F-actin domain (simple arrows in Fig. S5C′-D′). In *wwtr1*$^{-/-}$ oocytes at the same developmental stage, no MC was present at the animal pole (compare Fig. S5E with C). The FCL was homogeneous (yellow bracket) and not in contact with the oolemma, leaving a wide gap between the two layers (green bracket) as shown in Fig. 3R. Accordingly, no ZO-1 staining was observed at the oocyte animal pole surface (Fig. S5E′,F,F′). Viewing from the animal pole, the indentation of the oolemma was clearly visible (Fig. S5F,F′). This shows that TJs are present between the MC and the oolemma in control follicles and confirm the absence of MC in *wwtr1*$^{-/-}$ follicles.

TJs control the permeability of cell-cell contacts but have poor adhesive properties (Hartsock and Nelson, 2008). We therefore looked for the presence of adherens junctions (AJs) using E-cadherin and β-catenin antibodies. Whereas E-cadherin localized at the MC-oocyte contact point and as small aggregates in the cytoplasm at late stage III (white arrowhead in Fig. 5A), β-catenin was already clearly visible at the contact point at the beginning of stage III (white arrowhead in Fig. 5B). At this stage, it was also present at low levels at the lateral membrane of the MC (white arrows). In late stage III oocytes, β-catenin was still present at the MC-oocyte contact point (white arrowhead in Fig. 5C) but had delocalized from the lateral membrane and appeared as small aggregates in the MC cytoplasm, similar to E-cadherin (compare Fig. 5A with C). At both early and late stage III, β-catenin was detected at the interface between the FCs and the oocyte microvilli (yellow arrows in Fig. 5B,C). These results suggest that β-catenin and E-cadherin function in maintaining the adhesion between the MC and the oolemma in the stage III oocyte, and that during MC

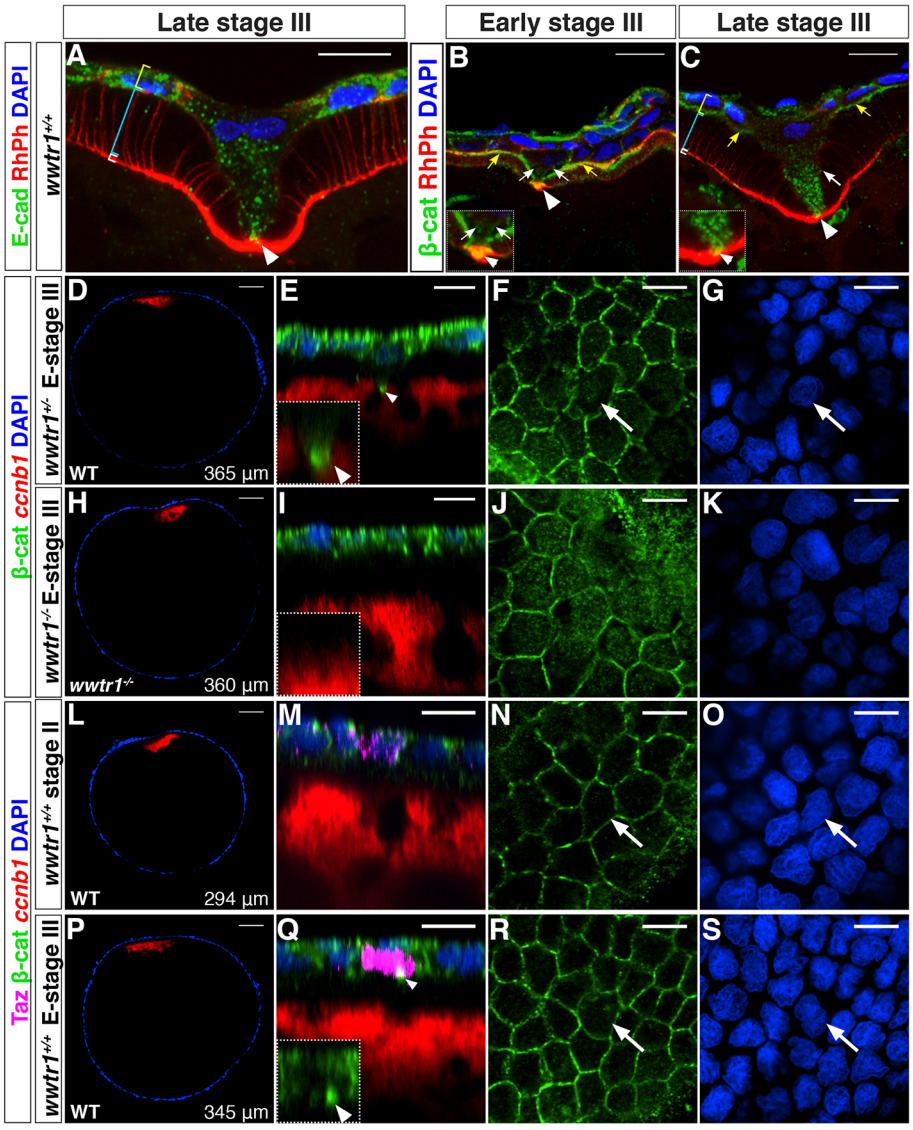

Fig. 5. Taz is enriched in the MC precursor before detectable morphological changes. (A-C) Single plane confocal images of cryosectioned ovaries showing E-cadherin (A, *n*=8) or β-catenin (B,C, *n*=10) localization in the MC and the neighboring FCs at the contact point (white arrowhead), at the MC membranes (white arrows) and at the interface between the oocyte microvilli and the FCs (yellow arrows). White, cyan and yellow brackets indicate the oocyte cortex, the microvilli/vitelline membrane and the FCL, respectively. Insets (B,C) are higher magnification views of the contact point. Rhodamine Phalloidin (RhPh) and DAPI were used to independently mark membranes and nuclei, respectively. (D-S) Confocal images of *wwtr1*$^{+/+}$, *wwtr1*$^{+/-}$ or *wwtr1*$^{-/-}$ whole-mount follicles at the indicated stage stained with Taz and/or β-catenin antibodies, *ccnb1* mRNA and DAPI as indicated. D,H,L,P are overview images with the follicle size indicated in the lower right corner. White arrowheads in E and Q point to β-catenin enrichment at the contact point; white arrows indicate an MC. E-stage III, early stage III. Scale bars: 10 µm in A-C,E-G,I-K, M-O,Q-S; 50 µm in D,H,L,P.

Development (2018) 145, dev167023. doi:10.1242/dev.167023

differentiation a ring of TJs additionally forms around the AJs between the MC and the oocyte surface.

Taz is enriched in the MC precursor before detectable morphological changes

To clarify when Taz is required in the formation of the MC, we analyzed whether morphological changes in the MC (e.g. increase in size, change in shape or establishment of a β-catenin-rich contact point with the oocyte surface) occur in the absence of Taz and whether they precede or follow Taz enrichment in the MC precursor.

Overview images of the follicles were taken to determine precisely the oocyte stage (Fig. 5D,H,L,P), and DAPI and β-catenin were used to label the FC nuclei (Fig. 5G,K,O,S) and cell membranes as well as the MC-oocyte contact point (Fig. 5F,J,N,R), respectively. As described earlier, at early stage III the MC has usually increased its size, changed its shape and established a β-catenin-rich contact point with the oocyte surface (arrowheads in Fig. 5E and Fig. S6A,B,D,F,G). Neither of these characteristics was present at the animal pole of stage-matched *wwtr1*$^{-/-}$ follicles (Fig. 5H-K). Similarly, in WT follicles at late stage II, the MC precursor in which Taz enrichment is just visible (Fig. 5M) is indistinguishable from its neighboring FCs based on its size, shape, nuclear morphology or β-catenin distribution (Fig. 5M-O, see also Fig. S6I,L).

Intriguingly, we observed MC precursors with clear Taz enrichment and β-catenin enrichment at their apical side (white arrowhead in Fig. 5Q) but with no or little changes in shape (Fig. 5R-S, see also Fig. S6J-M). In these cases, the β-catenin-rich apical tip is in contact with the microvilli of the oocyte, rather than with its surface (Fig. 5Q, Fig. S6J,M and Movie 1). Interestingly, in most of the WT late stage II to early stage III follicles we sampled (Fig. 5L-S and Fig. S6, 290-365 µm), either Taz was enriched in the MC precursor and β-catenin was concentrated at the apical tip (9/16, Fig. 5E,Q and Fig. S6A,B,D,F,G,J,M) or neither of these two traits was present (4/16, Fig. S6C,E,H,L). This suggests that these two events occur in a coordinated manner in a narrow time window. In a few cases, Taz was enriched but β-catenin was not yet concentrated at the apical tip (3/16, Fig. 5M and Fig. S6I,L) but we never observed β-catenin at the apical tip before Taz enrichment (0/16). Altogether, these experiments indicate that Taz starts to be enriched in the MC precursor before any observable change in cell size, shape or nuclear morphology (Fig. 5M-O). Following this, β-catenin concentrates at the apical part of the cell (arrowhead in Fig. 5Q) at the contact point with the oocyte microvilli (Movie 1). Finally the MC precursor extends an apical process and makes contact with the oolemma (white arrowhead, Fig. 5E). These results support an early role of Taz in the specification of the MC before morphological changes are visible and/or in driving the differentiation program of the MC.

Molecular characterization of the micropylar cell

As TJs and AJs are associated with the actomyosin cytoskeleton, we examined the temporal changes in the actomyosin organization at the contact point. To determine how non-muscle myosin II (NMII) is associated with the contact point at different stages of oogenesis, we used the *Tg(actb2:myl12.1-eGFP)* transgenic line that expresses the light chain of NMII fused to GFP (Maître et al., 2012). NMII was organized as a thin layer around the oocyte cortex together with F-actin in early stage III oocytes (see Fig. 6A for Myl12.1-gfp and Fig. 6D′ for F-actin). Intriguingly, as oogenesis proceeded, a NMII-free domain formed at the MC-oocyte contact zone (Fig. 6B, white bracket). This gap was specific to NMII as the actin cytoskeleton organization appeared uninterrupted (Fig. 6D′-F′). As the MC enlarged, the size of the NMII-free zone expanded and became much larger than the MC-oocyte contact point (Fig. 6C, white bracket). Such an NMII-free zone was not observed in the *wwtr1*$^{-/-}$ oocyte (Fig. S7A-B′), which suggests that it is a consequence of MC formation.

In the MC itself, the activated phosphorylated form of NMII (pNMII) localized at the membrane from early stage III of oogenesis onwards (Fig. 6D). At mid-stage III, when the MC extends dramatically in length, pNMII co-localized with F-actin at the lateral membrane of the MC (Fig. 6E,E′). At late stage III, however, once the MC was close to reaching its final size, both F-actin and activated NMII were barely detectable at the membrane (Fig. 6F, F′), similar to E-cadherin and β-catenin (Fig. 5A,C). This dynamic spatio-temporal distribution of NMII at the contact point and in the MC suggest that actomyosin-mediated tension could either be involved in or respond to the MC morphogenetic changes.

To further test this hypothesis, we exposed mid-stage III oocytes to the actin-severing drug cytochalasin D. Exposure to cytochalasin D strongly disorganized actin organization in the FCL, the oocyte and the microvilli (Fig. 6J-K). In comparison, the shape of the MC was mildly affected: although the MC process was often thin and misaligned with the cell body (Fig. 6L-M and Movie 2), the MC volume was unchanged (Fig. S7C), which suggests that additional cellular components maintain the shape of the MC.

Ultrastructural studies in Medaka and in the Chum Salmon have shown that the MC is particularly enriched in stable microtubules (Kobayashi and Yamamoto, 1985; Nakashima and Iwamatsu, 1989). From mid-stage III onward, stable microtubules, labeled with an antibody against acetylated Tubulin, were enriched at the tip of the cytoplasmic process (white arrow in Fig. 6H-I), which suggests that they might also play a structural role in the MC to promote its growth and resistance to extrinsic mechanical stress. To probe a functional role of stable microtubules, we incubated late stage III or early stage IV follicles at 4°C for 4 h (Tilney and Porter, 1967). Cold treatment efficiently destabilized stable microtubules (compare acetylated Tubulin signal in Fig. 6N and O). The shape of the MC was moderately affected (Fig. 6N,O and Fig. S7D,E). While neither the volume nor the height of the MC was significantly changed (Fig. S7D,E), the area of contact with the oolemma was slightly, but significantly, increased (Fig. 6P and Movie 3). In addition, the angle formed at the contact point between the MC process and the oolemma (dotted line in Fig. 6N-O) was significantly increased (Fig. 6Q), which suggests that stable microtubules in the MC process promote pushing on the oocyte surface.

In addition to stable MTs, intermediate filaments have been shown to be particularly enriched in the MC in other teleost species (Kobayashi and Yamamoto, 1985; Nakashima and Iwamatsu, 1989). Intriguingly, both the desmosomal marker desmoplakin (Dsp) and the intermediate filament component keratin 18 (Krt18) were specifically enriched in the MC compared with the rest of the FCs in stage III follicles (Fig. 7A-H). Dsp was present as aggregates in the entire MC cytoplasm and was enriched at the contact point with the oocyte surface (arrow in Fig. 7A-B′′). This localization was similar to β-catenin and E-cadherin localization (Fig. 5A-C). In contrast, Krt18 organized as a thick coat around the nucleus in the MC (Fig. 7C-H). In agreement with the fact that the MC does not form in *wwtr1*$^{-/-}$ follicles, both Dsp and Krt18 were absent (Fig. S8A-H). This result suggests that intermediate filaments could play a structural role to mechanically support the MC body during its elongation.

Development (2018) 145, dev167023. doi:10.1242/dev.167023

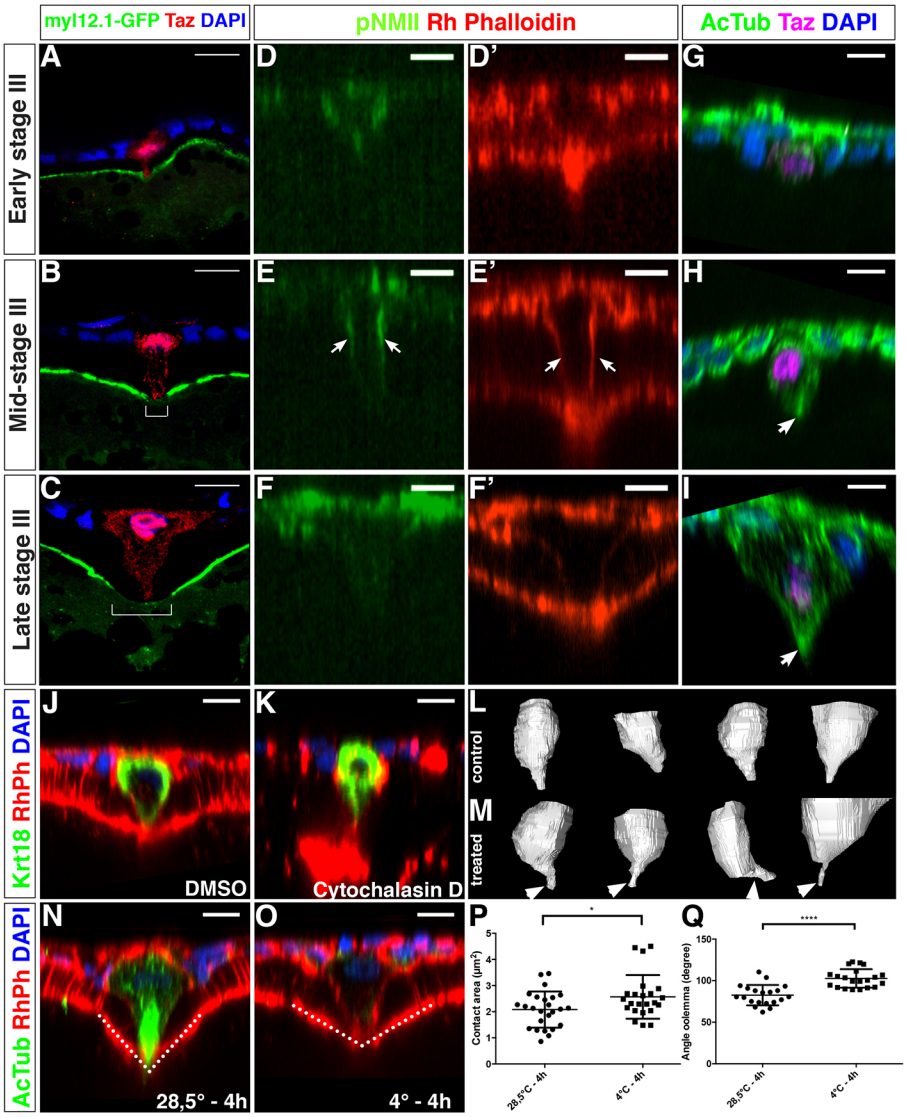

Fig. 6. Actomyosin and microtubule cytoskeleton organization the MC. (A-C) Single plane confocal images of cryosectioned ovaries displaying the temporal changes in the localization of Myl12.1-GFP at the animal cortex of the oocyte (*N*=2, *n*=34). During stage III, a zone with strongly reduced Myl12.1-GFP forms (white bracket in B,C). (D-E′) Orthogonal views of confocal stacks. Whole-mount follicles stained with an anti-pNMII and Rhodamine Phalloidin (*n*=27) at the indicated stages of oogenesis. Arrows in E,E' indicate the localization of pNMII and actin at the lateral membranes of the MC. Rhodamine Phalloidin is used to independently mark the MC membranes (D′-F′). (G-I) Whole-mount follicles stained with an anti-acetylated tubulin antibody to detect stable microtubules in the MC (arrow in H and I) (*n*=16). (J-O) Whole-mount follicles immunostained with Krt18 (J-K, see Fig. 7 and Results) or acetylated Tubulin (AcTub, N-O) antibodies and counterstained with Rhodamine Phalloidin (RhPh) and DAPI after either cytochalasin D treatment (K, DMSO control in J) (*N*=2, control *n*=19, treated *n*=19) or cold treatment (O, control in N) (*N*=3, control *n*=26, treated *n*=25). (L,M) Snapshots of 3D reconstruction of MCs (see Materials and Methods) from follicles treated with cytochalasin D (M) or with DMSO (L) (see also Movie 2). (P,Q) Quantification of the area of contact between the MC and the oocyte surface (P, *P*=0.032) or the angle formed at this point (Q, dotted line in N,O; *P*<0.0001, unpaired two-tailed *t*-tests). *N*, number of experiments; *n*, number of samples. Scale bars: 10 µm in A-O.

In summary, we have generated the first phenotypic map of MC morphogenesis at the molecular level. This characterization shows that the MC precursor, like all other FCs, is first in contact with the oocyte microvilli (Fig. 8A,B). Once Taz becomes enriched in one particular cell, this cell changes its β-catenin distribution, its shape and then directly contacts the oolemma via β-catenin/E-cadherin and Dsp-containing junctions (Fig. 8C,D). In addition, TJs reinforce the MC-oocyte link. Our data further point to a role of the actomyosin, microtubules and intermediate filaments cytoskeleton downstream of Taz to: actively drive the drastic changes in cell shape and size, to stabilize these changes and to provide the MC with mechanical resistance to pressure from the forming vitelline membrane, the neighboring FCs and the oocyte.

DISCUSSION

In this study, we show that females lacking the Hippo pathway effector Taz are infertile because their eggs lack a micropyle and thus cannot be fertilized by a sperm. We identify Taz as the first MC biomarker described to date and show that Taz enrichment in the future MC precedes changes in cell shape, size or adhesion properties. Finally, we perform the first molecular characterization of the MC in zebrafish and have identified two additional players that specifically differentiate the MC from other FCs: the intermediate filament component Krt18 and the desmosomal protein Dsp. Together, these results lead us to propose a hypothetical model of the role of Taz in the specification and differentiation of the MC (Fig. 8).

What is the nature of the signals required to specify a unique MC?

Analysis of the *buc* mutant phenotype clearly shows that the WT oocyte signals to the FCL to restrict the position of the MC (Marlow and Mullins, 2008). The nature of the signal, either biochemical or mechanical, and how it is transmitted from the oocyte to the FCL is, however, not yet known. Yet, a close-range signal or even direct cell contact, rather than a broadly diffusible signal, has been proposed (Heim et al., 2014). Previous studies have shown that the microvilli that extend from the surface of the zebrafish oocyte make direct contact with the adjacent follicle cells via β-catenin/E-cadherin-containing junctions, which mediate cell-cell adhesion (Cerdà et al., 1999). Here, we confirm this observation and show that the MC precursor is also in contact with microvilli before Taz becomes enriched in it (Figs 5M and 8A,E). Although the microvilli appear to be morphologically indistinguishable irrespective of oocyte polarity, the microvilli at the animal pole could have different

Development (2018) 145, dev167023. doi:10.1242/dev.167023

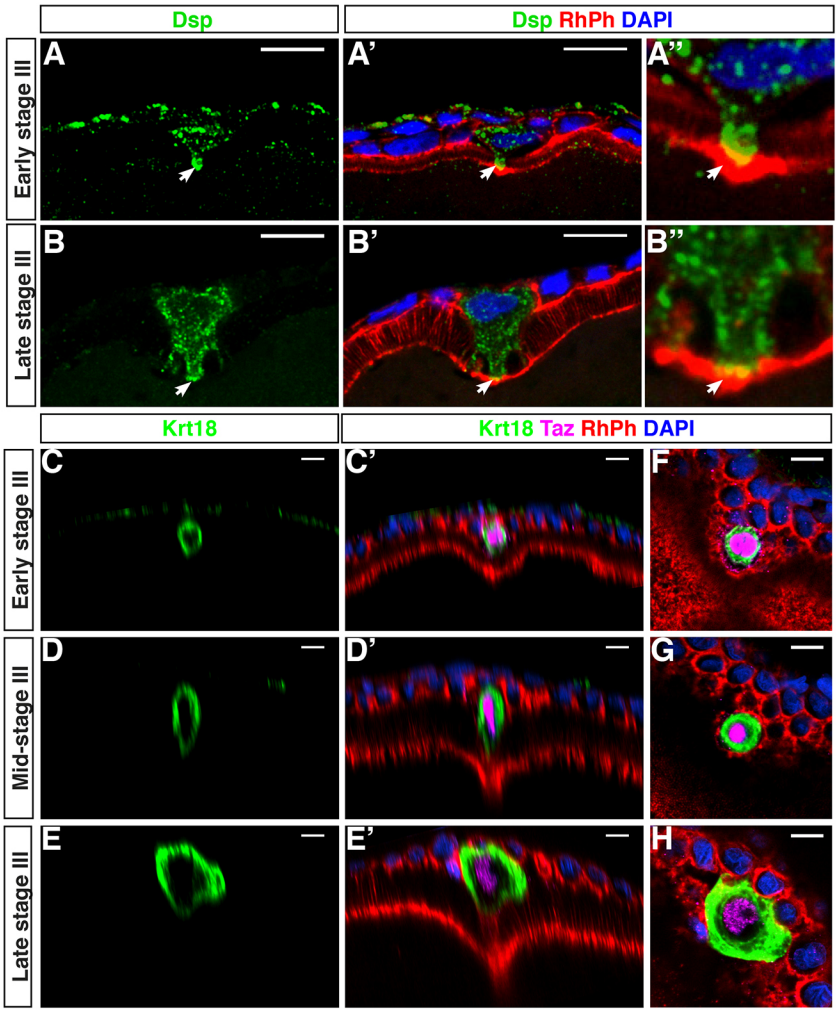

Fig. 7. Dsp and Krt18 are specifically enriched in the MC. (A-B′′) Confocal images of cryosectioned ovaries stained with an anti-desmoplakin antibody, Rhodamine Phalloidin (RhPh) and DAPI (*n*=13). White solid arrow points to the contact point between the MC and the oocyte. (C-H) Whole-mount immunofluorescence with an antibody against the intermediate filament protein Krt18 (*n*=11). C-E′ are orthogonal views of the confocal stacks shown in F-H. Taz antibody, DAPI and Rhodamine Phalloidin were used to counterstain the MC, the nuclei and membranes, respectively. Scale bars: 10 µm.

properties and transmit the signal from the oocyte animal pole to the future MC.

Several of our observations support this hypothesis. First, we show that immediately after Taz levels increase, β-catenin becomes specifically enriched at the contact point between these microvilli and the MC precursor (Fig. 5Q, Fig. S6J,M and Movie 1). This result alludes to the possibility that, before this enrichment, the microvilli at the animal pole mediate differential adhesion. Second,

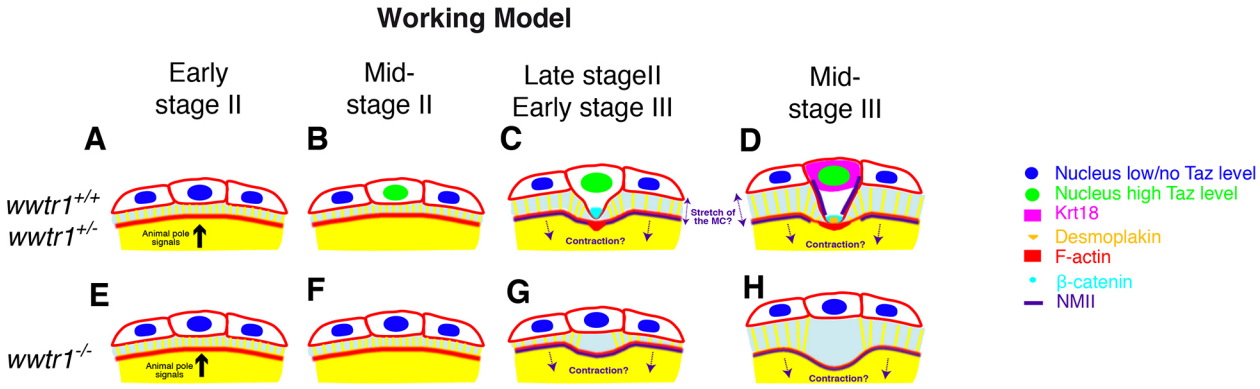

Fig. 8. Working model of the micropylar cell fate acquisition. (A-D) Working model based on the results obtained in the present study (see also Discussion). We propose that signals from the animal pole of the oocyte are transmitted to the overlying FCL leading to an increase in Taz level in the closest cell, the MC precursor (A,B). This leads to the enrichment of β-catenin at the apical tip and to changes in growth and shape (B). In early stage III, the MC, via its β-catenin-rich apical tip, enters into contact with and attaches to the oolemma. Simultaneously, the microvilli around the oocyte lengthen and the space between the oolemma and the FCL increases, leading to stretching of the MC (C). Krt18-containing intermediate filaments and stable microtubules participate to the MC differentiation and stabilization (D). (E-H) In the *wwtr1*$^{-/-}$ follicles, although the signals from the animal pole are unchanged (E), none of the changes that occur in the WT MC precursor occur in the absence of Taz function (F-H). The microvilli at the animal pole fail to adhere to the overlying FC and/or autonomously regress, leading to the formation of a large gap between the oolemma and the FCL in place of the MC (G-H).

Development (2018) 145, dev167023. doi:10.1242/dev.167023

the animal pole microvilli behave differently from the rest of the microvilli at later stages of oogenesis. At stage IV of oogenesis, microvilli from the FCs and from the oocyte retract to prepare for ovulation (Selman et al., 1993). Our observations indicate that the microvilli at the animal pole regress much earlier, to enable the attachment of the MC to the oolemma (Figs 3Q, 5A,C and 8C). Surprisingly, animal pole microvilli are also absent in *wwtr1*$^{-/-}$ oocytes (Figs 3R, S5E, and 8G,H), supporting the idea that this loss is independent of the MC growth and is autonomous to the microvilli at the animal pole.

Furthermore, if the animal pole microvilli were identical to the rest of the microvilli, they would attach to the FC at the animal pole in *wwtr1*$^{-/-}$ follicles, which fail to acquire an MC fate. Instead, we observe a large gap between the FCL and the oolemma in place of the MC in *wwtr1*$^{-/-}$ follicles (Figs 3R, S5E and Fig. 8G,H). This indicates a complete loss of adhesion and attachment, which is compatible with the hypothesis that the microvilli at the animal pole have different adhesive properties compared with the rest of the microvilli. This loss of attachment could also explain the indentation we often observe at the surface of the oocyte in *wwtr1*$^{-/-}$ follicles (Figs 3P,R, S3E,G and S5E): if the oolemma is not attached to the apical surface of the FCs, it flops down.

The activity of Yap and Taz is known to be regulated by diverse intrinsic and extrinsic cues, including mechanical forces, cell polarity and cell adhesion (reviewed by Elbediwy and Thompson, 2018; Halder et al., 2012; Sasaki, 2015). Therefore differential properties of the microvilli at the animal pole, e.g. differential adhesion, could induce the enrichment of Taz in the future MC (Kim et al., 2011; Schlegelmilch et al., 2011; Yang et al., 2015). Taz enrichment is rapidly followed by a concentration of β-catenin at the MC precursor-microvilli contact point (Fig. 5 and Movie 1). This would enhance the differential adhesion and could therefore work as a positive feedback loop, promoting the strong increase in Taz levels we observe in the MC precursor (Fig. 8B-D).

After Taz levels starts to increase within it, the MC precursor changes its shape, grows and acquires an MC process that directly contacts the oocyte surface via β-catenin/E-cadherin/Dsp-containing junctions (Figs 5A,C, 7A,B and 8C,D). Simultaneously, the microvilli that separate the oocyte and the other FCs grow (compare Figs 5B with C, and 7A′ with B′), thus increasing the distance between the oocyte surface and the FCL (Selman et al., 1993). This most likely induces tension on the MC lateral membrane (Fig. 8C,D). Accordingly, actin and activated NMII levels transiently increase along the elongated MC lateral membrane in mid-stage III follicles (Fig. 6E,E′). We propose that this elongation of the MC and increase in tension, combined with the attachment of the MC to the oolemma (see previous paragraph), contribute to sustained Taz enrichment in the MC.

Finally, we report the presence of a cortical actomyosin network surrounding the oocyte beneath its surface (Fig. 6A). This raises the possibility that the oocyte cortex is contractile and capable of generating pulling forces (Fig. 8C,D). Although this hypothesis needs to be tested experimentally, such contractile forces, combined with the adhesion between the oocyte and the MC precursor, could contribute to the sustained enrichment of Taz in this specific cell. Based on our results, we propose that once β-catenin-mediated contact between the oolemma and the MC is established, downstream of Taz enrichment, the growth of surrounding microvilli, as well as contractile forces from the oocyte, could all contribute to maintaining Taz levels higher in the MC and also facilitate its nuclear translocation (Fig. 8A-D). The observation that both a TEAD reporter and CTGF are specifically enriched in the MC (Fig. 4L′,O′ and Fig. S4C) indicates that Taz functions as a TEAD-dependent transcription effector in the MC and likely induces the expression of genes that are required for the growth and differentiation of the MC. Future genome-wide expression profile studies emerge as a promising approach to identify Taz target genes that mediate MC differentiation.

What are the events downstream of Taz that drive the differentiation of the MC?

Which cellular events are activated downstream of Taz, that make an FC differentiate into the very specialized MC? There are two major differences between these two related cell types: their size and their shape. Concerning the increase in size, two factors that are implicated in cell growth regulation are the transcription factor Myc and the mTOR signaling pathway (reviewed by Lloyd, 2013). Interestingly, in *Drosophila* Myc has been shown to function as a critical effector of cellular growth downstream of Yki, the homolog of Yap/Taz (Neto-Silva et al., 2010). Similarly, several studies have shown that the Hippo-YAP pathway acts as an upstream regulator of mTOR and that these two pathways coordinate to control cell size and growth (James et al., 2009; Liu et al., 2017; López-Lago et al., 2009; Santinon et al., 2016; Tumaneng et al., 2012). It will therefore be interesting to investigate whether the strong increase in size of the MC is due to an increase in Myc or mTOR activity downstream of Taz. Interestingly, keratin cytoskeletal proteins, including Krt18, regulate protein synthesis and cell growth upstream of the Akt/mTOR signaling pathway in keratinocytes (Kim et al., 2006). Since we show here that Krt18 is specifically and highly enriched in the MC, Krt18 might be involved in the large increase in size of the MC.

In addition to the obvious increase in size, the MC acquires a very characteristic mushroom-like shape during its morphogenesis. Cell shape changes are often associated with dynamic properties of the actomyosin cytoskeleton (reviewed by Murrell et al., 2015; Rauzi and Lenne, 2011; Salbreux et al., 2012). Here, in contrast, we show that the destabilization of actin filaments does not strongly affect the shape of MCs (Fig. 6J-M and Fig. S7C). This could be because MC morphogenesis is a much slower process than changes in cell shape during developmental processes. Moreover, our results suggest that both stable MTs (Fig. 6G-I,N-Q and Fig. S7D-E) and intermediate filaments (Fig. 7A-H) could also play a structural role in establishing and maintaining the shape of the MC. One of the main functions of intermediate filaments is, indeed, to provide mechanical strength, including plasma membrane support in diverse cell types (reviewed by Loschke et al., 2015; Quinlan et al., 2017). We thus propose that intermediate filaments provide mechanical strength to support the MC plasma membrane in withstanding the pressure from the forming vitelline membrane over this longer time period.

MATERIALS AND METHODS

Zebrafish husbandry

Procedures involving animals were conducted according to the guidelines of Goethe University in Frankfurt, Germany and approved by the German authorities (veterinary department of the Regional Board of Darmstadt). The previously characterized mutant *taz*^{mw49} (Miesfeld et al., 2015), and the transgenic *Tg(4xGTIIC-d2EGFP)*^{mw50} (Miesfeld and Link, 2014) and *Tg(actb2:myl12.1-eGFP)*^{e2212Tg} (Maître et al., 2012) lines were used in this study.

Generation of mutant and transgenic zebrafish lines

The mutant line *wwtr1*^{fu55} was generated using TALEN-induced mutagenesis strategy as previously described (Agarwala et al., 2015). Several mutant alleles were recovered using PCR by amplifying a region

Development (2018) 145, dev167023. doi:10.1242/dev.167023

that encompassed the target site, using the primers *wwtr1-tal1-e1-fow* and *wwtr1-tal1-e1-rev* (Table S3) and digesting it with *Bsp*HI. Zygotic mutants obtained from an incross of heterozygous mutant fish were raised to adulthood to obtain F3 maternal-zygotic (MZ) mutants.

The *zp0.5:eGFP-zorba* and *bactin2:lyntdt* transgenes were generated by amplifying the *−0.5zp3b* and *bactin2* promoters from plasmids *−0.5zp3b:GFP* and *p5E-bactin2*, respectively (Kwan et al., 2007; Onichtchouk et al., 2003) and cloning them into a vector containing recognition sites for the Tol2 transposase. Full-length *zorba* (*cpeb1b*) cDNA was amplified from total zebrafish cDNA and cloned into the vector containing the *−0.5zp3b* promoter and the Tol2 sites (for primer, see Table S3). The construct was injected at a concentration of 40 ng/µl along with the transposase mRNA (50 ng/µl). Transposase mRNA was synthesized with the mMessage mMachine Sp6 Polymerase Kit (Ambion) from pCS2FA-transposase (Kwan et al., 2007). Positive oocytes expressing the eGFP-Zorba fusion protein were isolated from founder F0 females (Fig. S3A-D). Positive F1 could not be recovered, which suggests that the transgene was already silenced in the first generation. Therefore only oocytes from F0 females were used.

Mature egg activation and IVF

Mature eggs were obtained by gently squeezing the belly of gravid females and were activated in E3 medium. The micropyle was then either observed directly or stained with Coomassie Brilliant Blue (Yanagimachi et al., 2013). IVF was performed according to standard protocols (Westerfield, 2007). IVF on dechorionated eggs was performed with the following alterations. Activated unfertilized eggs were incubated in a glass dish with 0.5 mg/ml Pronase-E3 under visual control and immediately transferred into a large beaker filled with E3 as soon as the first eggs were leaving the chorion. After gentle swirling, dechorionated eggs were placed into agarose-coated petri dishes prefilled with E3. Excess E3 was removed and IVF was initiated by adding 250 µl sperm solution (pooled sperm from two WT males) followed 1 min later by 1-2 ml 0.5% fructose-E3 for a further 2 min, before filling the dish with E3.

Ovary dissection and immunostaining on cryosections

Adult zebrafish were euthanized using an overdose of tricaine, according to the institutional guidelines approved by the German authorities. The ovary was dissected out of freshly euthanized females using a sharp pair of forceps. The ovarian tissue was quickly rinsed in L-15 medium (pH 9) (Gibco, 31415-029) and then used for further processing.

For cryosections, dissected ovaries were fixed with 4% paraformaldehyde (PFA) in PBS (pH 7.4) overnight at 4°C and washed with PBS 5× for 5 min each. Whole ovaries were then transferred to the following solutions and allowed to equilibrate for one day: 25% sucrose in PBS, 35% sucrose in PBS, 1:1 optimal cutting temperature compound (OCT) (TissueTek): 35% sucrose in PBS and 100% OCT. The ovaries were then transferred to a mold containing fresh OCT and frozen on a metal block that was stored at −80°C. A cryotome was used to obtain 10 µm cryosections, with the block at −15°C and the chamber at −20°C, which were placed on Superfrost UltraPlus slides (Thermo Scientific, J3800AMNZ) and air-dried at room temperature (RT) for at least 2 h and then stored at −80°C.

Ovary dissection, cytochalasin D treatment and cold treatment

Ovaries were dissected and follicles of desired stages were manually separated. Cytochalasin D and cold treatment were performed for 4 h. We used 1% DMSO as a control for cytochalasin D (2 µg/ml) in 3 ml of 90% L-15 medium containing 0.5% bovine serum albumin (BSA) (pH 9). For cold treatment, follicles in 90% L-15 medium with 0.5% BSA (pH 9) were incubated either at 28.5°C (controls) or at 4°C for 4 h.

Oocyte isolation and fixation for whole-mount immunostaining and in situ hybridization

Dissected ovaries were digested with collagenase (0.25 mg/ml) for 10 min and individual ovarian follicles were gently dissociated using a cut 1 ml pipette tip. Dissociated follicles were washed with L-15 medium (pH 9) 3-4 times. L-15 medium was removed completely and follicles were acid-fixed overnight at 4°C or for 2 h at RT with 2 ml of 5% formaldehyde in PBS and 8-10 drops of glacial acetic acid (1 drop is approximately 50 µl, final concentration of the acid ∼5%-8%) (Fernández and Fuentes, 2013). Fixed follicles were washed 5× with PBS containing 0.1% Tween-20 (PBST). In Fig. 6 (pNMII/Phalloidin staining), ovarian follicles were fixed in 4% PFA in PBS overnight at 4°C.

Acid-fixed or PFA-fixed follicles were blocked with PBDT-I [1× PBS, 1% BSA, 1% dimethyl sulfoxide (DMSO) and 0.5% Triton X-100] containing 2% normal goat serum (NGS) for at least 30 min. Follicles were incubated in primary and secondary antibodies either overnight at 4°C or for 4 h at RT. After antibody incubation, the follicles were washed 5× for 20 min in PBDT-I. The following antibodies were used: mouse anti-β-catenin (1:200, Sigma-Aldrich, C7207), rabbit anti-Taz (1:200, Cell Signaling Technology, D24E4) (Miesfeld et al., 2015), mouse anti-acetylated tubulin (1:200, Sigma-Aldrich, T6793), mouse anti-Desmoplakin (ready to use, Progen, 651155), mouse anti-Krt18 (1:200, Thermo Fisher Scientific, MA1-06326), rabbit anti-pNMII (1:50, Cell Signaling Technology, 3671S), mouse anti-GFP (1:500, Clontech Laboratories, 632381), rabbit anti-GFP (1:500; Torrey Pines Biolabs, TP401), mouse anti-E-Cad (1:200, BD Biosciences, 610182), rabbit anti-CTGF (1:200, Abcam, ab6992; Merkes et al., 2015) and mouse anti-ZO1 (1:500; Invitrogen, 33-9100). Alexa 488/568/647-conjugated antibodies (Thermo Fisher Scientific) were used at 1:500 dilution. Immunofluorescence on cryosections was performed according to the protocol published on Abcam's website (www.abcam.com/protocols/immunostaining-paraffin-frozen-free-floating-protocol). Rhodamine Phalloidin (Molecular Probes, R415) was used at 1:100 dilution. The sections were blocked in 5% NGS in PBDT-II (1× PBS, 1% BSA, 1% DMSO and 0.025% Triton X-100) and all the washes were performed with PBDT-II.

As many antibodies do not work after *in situ* hybridization (ISH), this procedure was performed after immunostaining on acid-fixed ovarian follicles whenever necessary (Elkouby and Mullins, 2016). Immunostained follicles were post-fixed in 4% PFA in PBS for 20 min at RT followed by washing 5× for 5 min each in PBST. ISH was then performed according to standard protocol starting at the prehybridization stage (Thisse and Thisse, 2008). Hybridization was performed at 60°C overnight. The following probes and antibodies were used: *cyclinb1* (1:200) (Kondo et al., 1997) to mark the animal pole, *dazl* (1:200) to mark the vegetal pole and the Balbiani Body (Kosaka et al., 2007). For single WISH, probes were DIG labeled (DIG RNA Labeling Mix, Roche, 11277073910) and detected with an anti-DIG-AP (1:400, Roche, 11093274910) antibody and FastRed (Roche, 11496549001) as a substrate in 0.1 M Tris buffer with 0.1% Tween-20 (pH 8.2).

For double fluorescent WISH, a fluorescein-labeled *ccnb1* probe was used in combination with DIG-labeled *dazl1*. After the fixation/permeabilization step, endogenous horseradish peroxidase (HRP), was quenched with 1% H_2O_2 in PBST. To detect the fluorescein-labeled RNA, anti-HRP antibody (1:150, Perkin Elmer, NEF710) was used. Tyramide-Alexa488 substrate was used to localize the *ccnb1* transcripts [1:50 in provided buffer, Perkin Elmer, FP1134 (buffer), FP1168 (substrate)].

Microscopy and image processing

Ovarian follicles were staged according to Selman et al. (1993). Individual follicles were mounted on 24×60 mm coverslips in a 0.8% low-melting agarose drop diluted in E3 medium. Imaging was performed on a Nikon W1 Spinning Disc Microscope with the following objectives: 10× air objective (NA 0.45, WD 4 mm), or 20× (NA 0.95, WD 0.95 mm), 40× (NA 1.15, WD 0.60 mm) and 60× (NA 1.20, WD 0.30 mm) water objectives. Images were processed using the Fiji software. For 3D segmentation, the semi-automatic segmentation plugin 'segmentation editor' was used. Later, the segmented image was uploaded into the Fiji 3D ROI manager to further quantify volume and feret (Ollion et al., 2013). Feret is the longest distance between any two points in a selected ROI.

Statistical analysis

Statistical analyses were performed using GraphPad Prism and unpaired two-tailed *t*-tests were performed to calculate *P* values. In graphs, data are represented as mean±s.e.m. *P* values are indicated in the respective figure legends: *P<0.05, **<0.01, ***<0.001.

RNA extraction, cDNA synthesis and RT-PCR

Total RNA was extracted with Trizol from samples collected at the following developmental stages: unactivated eggs, 256-cell stage, sphere, 60% epiboly and 28 h postfertilization. We reverse-transcribed 1 µg of total RNA using Superscript III (Invitrogen). Primer sequences for RT-PCR are provided in Table S1.

Acknowledgements

We are grateful to Sabine Götter in Prof. Wolfgang Driever's laboratory (Freiburg), Denise Werner and Tore Dittrich (Frankfurt) for excellent fish care. We thank Daria Onichtchouk for valuable input at the beginning of the project, David Kleinhans for help with image analysis, Sarah Herberg and Andrea Pauli for their advice on the IVF on dechorionated eggs protocol, Carl-Philipp Heisenberg and Brian Link for zebrafish lines and Stefan Eimer for critical reading of the manuscript.

Competing interests

The authors declare no competing or financial interests.

Author contributions

Conceptualization: C.D., V.L.; Methodology: C.D., A.N., P.A.K., R.F., M.C.M.; Validation: C.D.; Formal analysis: C.D., P.A.K., R.F., M.C.M., V.L.; Investigation: C.D., A.N., P.A.K., S.G., R.F.; Resources: R.F., M.C.M.; Writing - original draft: C.D., V.L.; Writing - review & editing: C.D., P.A.K., R.F., M.C.M., V.L.; Visualization: C.D.; Supervision: V.L.; Project administration: V.L.; Funding acquisition: M.C.M., V.L.

Funding

This work was funded by the Deutsche Forschungsgemeinschaft (DFG-GRK1104 to C.D. and SPP1782 project number LE2681 to C.D. and V.L.) and the National Institutes of Health (R01GM117981 to M.C.M.). Deposited in PMC for release after 12 months.

Supplementary information

Supplementary information available online at
http://dev.biologists.org/lookup/doi/10.1242/dev.167023.supplemental

References

Agarwala, S., Duquesne, S., Liu, K., Boehm, A., Grimm, L., Link, S., König, S., Eimer, S., Ronneberger, O. and Lecaudey, V. (2015). Amotl2a interacts with the Hippo effector Yap1 and the Wnt/β-catenin effector Lef1 to control tissue size in zebrafish. *Elife* **4**, e08201.

Beyer, T. A., Weiss, A., Khomchuk, Y., Huang, K., Ogunjimi, A. A., Varelas, X. and Wrana, J. L. (2013). Switch Enhancers Interpret TGF-β and Hippo Signaling to Control Cell Fate in Human Embryonic Stem Cells. *Cell Rep.* **5**, 1611-1624.

Bontems, F., Stein, A., Marlow, F. L., Lyautey, J., Gupta, T., Mullins, M. C. and Dosch, R. (2009). Bucky ball organizes germ plasm assembly in zebrafish. *Curr. Biol.* **19**, 414-422.

Cerdà, J., Reidenbach, S., Prätzel, S. and Franke, W. W. (1999). Cadherin-catenin complexes during zebrafish oogenesis: heterotypic junctions between oocytes and follicle cells. *Biol. Reprod.* **61**, 692-704.

Dong, J., Feldmann, G., Huang, J., Wu, S., Zhang, N., Comerford, S. A., Gayyed, M. F., Anders, R. A., Maitra, A. and Pan, D. (2007). Elucidation of a universal size-control mechanism in Drosophila and mammals. *Cell* **130**, 1120-1133.

Elbediwy, A. and Thompson, B. J. (2018). Evolution of mechanotransduction via YAP/TAZ in animal epithelia. *Curr. Opin. Cell Biol.* **51**, 117-123.

Elkouby, Y. M. and Mullins, M. C. (2016). Methods for the analysis of early oogenesis in zebrafish. *Dev. Biol.* **430**, 310-324.

Elkouby, Y. M., Jamieson-Lucy, A. and Mullins, M. C. (2016). Oocyte polarization is coupled to the chromosomal bouquet, a conserved polarized nuclear configuration in meiosis. *PLoS Biol.* **14**, e1002335.

Fernández, J. and Fuentes, R. (2013). Fixation/permeabilization: new alternative procedure for immunofluorescence and mRNA in situ hybridization of vertebrate and invertebrate embryos. *Dev. Dyn.* **242**, 503-517.

Halder, G., Dupont, S. and Piccolo, S. (2012). Transduction of mechanical and cytoskeletal cues by YAP and TAZ. *Nat. Rev. Mol. Cell Biol.* **13**, 591-600.

Hart, N. H. and Donovan, M. (1983). Fine structure of the chorion and site of sperm entry in the egg of Brachydanio. *J. Exp. Zool.* **227**, 277-296.

Hartsock, A. and Nelson, W. J. (2008). Adherens and tight junctions: structure, function and connections to the actin cytoskeleton. *Biochim. Biophys. Acta* **1778**, 660-669.

Heim, A. E., Hartung, O., Rothhämel, S., Ferreira, E., Jenny, A. and Marlow, F. L. (2014). Oocyte polarity requires a Bucky ball-dependent feedback amplification loop. *Development* **141**, 842-854.

Hirate, Y., Hirahara, S., Inoue, K.-I., Suzuki, A., Alarcon, V. B., Akimoto, K., Hirai, T., Hara, T., Adachi, M., Chida, K. et al. (2013). Polarity-dependent distribution of angiomotin localizes Hippo signaling in preimplantation embryos. *Curr. Biol.* **23**, 1181-1194.

Howley, C. and Ho, R. K. (2000). mRNA localization patterns in zebrafish oocytes. *Mech. Dev.* **92**, 305-309.

Huang, J., Wu, S., Barrera, J., Matthews, K. and Pan, D. (2005). The Hippo signaling pathway coordinately regulates cell proliferation and apoptosis by inactivating Yorkie, the Drosophila homolog of YAP. *Cell* **122**, 421-434.

James, M. F., Han, S., Polizzano, C., Plotkin, S. R., Manning, B. D., Stemmer-Rachamimov, A. O., Gusella, J. F. and Ramesh, V. (2009). NF2/merlin is a novel negative regulator of mTOR complex 1, and activation of mTORC1 is associated with meningioma and schwannoma growth. *Mol. Cell. Biol.* **29**, 4250-4261.

Judson, R. N., Tremblay, A. M., Knopp, P., White, R. B., Urcia, R., De Bari, C., Zammit, P. S., Camargo, F. D. and Wackerhage, H. (2012). The Hippo pathway member Yap plays a key role in influencing fate decisions in muscle satellite cells. *J. Cell Sci.* **125**, 6009-6019.

Kim, S., Wong, P. and Coulombe, P. A. (2006). A keratin cytoskeletal protein regulates protein synthesis and epithelial cell growth. *Nature* **441**, 362-365.

Kim, N.-G., Koh, E., Chen, X. and Gumbiner, B. M. (2011). E-cadherin mediates contact inhibition of proliferation through Hippo signaling-pathway components. *Proc. Natl. Acad. Sci. USA.* **108**, 11930-11935.

Kobayashi, W. and Yamamoto, T. S. (1985). Fine structure of the micropylar cell and its change during oocyte maturation in the chum salmon, oncorhynchus keta. *J. Morphol.* **184**, 263-276.

Kondo, T., Yanagawa, T., Yoshida, N. and Yamashita, M. (1997). Introduction of cyclin B induces activation of the maturation-promoting factor and breakdown of germinal vesicle in growing zebrafish oocytes unresponsive to the maturation-inducing hormone. *Dev. Biol.* **190**, 142-152.

Kosaka, K., Kawakami, K., Sakamoto, H. and Inoue, K. (2007). Spatiotemporal localization of germ plasm RNAs during zebrafish oogenesis. *Mech. Dev.* **124**, 279-289.

Kwan, K. M., Fujimoto, E., Grabher, C., Mangum, B. D., Hardy, M. E., Campbell, D. S., Parant, J. M., Yost, H. J., Kanki, J. P. and Chien, C.-B. (2007). The Tol2kit: a multisite gateway-based construction kit for Tol2 transposon transgenesis constructs. *Dev. Dyn.* **236**, 3088-3099.

Leung, C. Y. and Zernicka-Goetz, M. (2013). Angiomotin prevents pluripotent lineage differentiation in mouse embryos via Hippo pathway-dependent and -independent mechanisms. *Nat. Commun.* **4**, 2251.

Liu, P., Calvisi, D. F., Kiss, A., Cigliano, A., Schaff, Z., Che, L., Ribback, S., Dombrowski, F., Zhao, D. and Chen, X. (2017). Central role of mTORC1 downstream of YAP/TAZ in hepatoblastoma development. *Oncotarget* **8**, 73433-73447.

Lloyd, A. C. (2013). The regulation of cell size. *Cell* **154**, 1194-1205.

López-Lago, M. A., Okada, T., Murillo, M. M., Socci, N. and Giancotti, F. G. (2009). Loss of the tumor suppressor gene NF2, encoding merlin, constitutively activates integrin-dependent mTORC1 signaling. *Mol. Cell. Biol.* **29**, 4235-4249.

Loschke, F., Seltmann, K., Bouameur, J.-E. and Magin, T. M. (2015). Regulation of keratin network organization. *Curr. Opin. Cell Biol.* **32**, 56-64.

Maegawa, S., Yasuda, K. and Inoue, K. (1999). Maternal mRNA localization of zebrafish DAZ-like gene. *Mech. Dev.* **81**, 223-226.

Maître, J.-L., Berthoumieux, H., Krens, S. F. G., Salbreux, G., Jülicher, F., Paluch, E. and Heisenberg, C.-P. (2012). Adhesion functions in cell sorting by mechanically coupling the cortices of adhering cells. *Science* **338**, 253-256.

Marlow, F. L. and Mullins, M. C. (2008). Bucky ball functions in Balbiani body assembly and animal-vegetal polarity in the oocyte and follicle cell layer in zebrafish. *Dev. Biol.* **321**, 40-50.

Merkes, C., Turkalo, T. K., Wilder, N., Park, H., Wenger, L. W., Lewin, S. J. and Azuma, M. (2015). Ewing sarcoma ewsa protein regulates chondrogenesis of Meckel's cartilage through modulation of Sox9 in zebrafish. *PLoS ONE* **10**, e0116627.

Miesfeld, J. B. and Link, B. A. (2014). Establishment of transgenic lines to monitor and manipulate Yap/Taz-Tead activity in zebrafish reveals both evolutionarily conserved and divergent functions of the Hippo pathway. *Mech. Dev.* **133**, 177-188.

Miesfeld, J. B., Gestri, G., Clark, B. S., Flinn, M. A., Poole, R. J., Bader, J. R., Besharse, J. C., Wilson, S. W. and Link, B. A. (2015). Yap and Taz regulate retinal pigment epithelial cell fate. *Development* **142**, 3021-3032.

Murrell, M., Oakes, P. W., Lenz, M. and Gardel, M. L. (2015). Forcing cells into shape: the mechanics of actomyosin contractility. *Nat. Rev. Mol. Cell Biol.* **16**, 486-498.

Musah, S., Wrighton, P. J., Zaltsman, Y., Zhong, X., Zorn, S., Parlato, M. B., Hsiao, C., Palecek, S. P., Chang, Q., Murphy, W. L. and Kiessling, L. L. (2014). Substratum-induced differentiation of human pluripotent stem cells reveals the coactivator YAP is a potent regulator of neuronal specification. *Proc. Natl. Acad. Sci. USA* **111**, 13805-13810.

Nakashima, S. and Iwamatsu, T. (1989). Ultrastructural changes in micropylar cells and formation of the micropyle during oogenesis in the medaka Oryzias latipes. *J. Morphol.* **202**, 339-349.

Neto-Silva, R. M., de Beco, S. and Johnston, L. A. (2010). Evidence for a growth-stabilizing regulatory feedback mechanism between Myc and Yorkie, the Drosophila homolog of Yap. *Dev. Cell* **19**, 507-520.

Nishioka, N., Inoue, K.-I., Adachi, K., Kiyonari, H., Ota, M., Ralston, A., Yabuta, N., Hirahara, S., Stephenson, R. O., Ogonuki, N. et al. (2009). The Hippo

signaling pathway components Lats and Yap pattern Tead4 activity to distinguish mouse trophectoderm from inner cell mass. *Dev. Cell* **16**, 398-410.
Ollion, J., Cochennec, J., Loll, F., Escudé, C. and Boudier, T. (2013). TANGO: a generic tool for high-throughput 3D image analysis for studying nuclear organization. *Bioinformatics* **29**, 1840-1841.
Onichtchouk, D., Aduroja, K., Belting, H.-G., Gnügge, L. and Driever, W. W. (2003). Transgene driving GFP expression from the promoter of the zona pellucida gene zpc is expressed in oocytes and provides an early marker for gonad differentiation in zebrafish. *Dev. Dyn.* **228**, 393-404.
Pan, D. (2007). Hippo signaling in organ size control. *Genes Dev.* **21**, 886-897.
Poleo, G. A., Denniston, R. S., Reggio, B. C., Godke, R. A. and Tiersch, T. R. (2001). Fertilization of eggs of zebrafish, Danio rerio, by intracytoplasmic sperm injection. *Biol. Reprod.* **65**, 961-966.
Quinlan, R. A., Schwarz, N., Windoffer, R., Richardson, C., Hawkins, T., Broussard, J. A., Green, K. J. and Leube, R. E. (2017). A rim-and-spoke hypothesis to explain the biomechanical roles for cytoplasmic intermediate filament networks. *J. Cell Sci.* **130**, 3437-3445.
Rauzi, M. and Lenne, P.-F. (2011). Cortical forces in cell shape changes and tissue morphogenesis. *Curr. Top. Dev. Biol.* **95**, 93-144.
Salbreux, G., Charras, G. and Paluch, E. (2012). Actin cortex mechanics and cellular morphogenesis. *Trends Cell Biol.* **22**, 536-545.
Santinon, G., Pocaterra, A. and Dupont, S. (2016). Control of YAP/TAZ activity by metabolic and nutrient-sensing pathways. *Trends Cell Biol.* **26**, 289-299.
Sasaki, H. (2015). Position- and polarity-dependent Hippo signaling regulates cell fates in preimplantation mouse embryos. *Semin. Cell Dev. Biol.* **47-48**, 80-87.
Schlegelmilch, K., Mohseni, M., Kirak, O., Pruszak, J., Rodriguez, J. R., Zhou, D., Kreger, B. T., Vasioukhin, V., Avruch, J., Brummelkamp, T. R. et al. (2011). Yap1 acts downstream of α-catenin to control epidermal proliferation. *Cell* **144**, 782-795.
Selman, K., Wallace, R. A., Sarka, A. and Qi, X. (1993). Stages of oocyte development in the zebrafish, brachydanio rerio. *J. Morphol.* **218**, 203-224.
Thisse, C. and Thisse, B. (2008). High-resolution in situ hybridization to whole-mount zebrafish embryos. *Nat. Protoc.* **3**, 59-69.
Tilney, L. G. and Porter, K. R. (1967). Studies on the microtubules in heliozoa. II. The effect of low temperature on these structures in the formation and maintenance of the axopodia. *J. Cell Biol.* **34**, 327-343.
Tumaneng, K., Schlegelmilch, K., Russell, R. C., Yimlamai, D., Basnet, H., Mahadevan, N., Fitamant, J., Bardeesy, N., Camargo, F. D. and Guan, K.-L. L. (2012). YAP mediates crosstalk between the Hippo and PI(3)K–TOR pathways by suppressing PTEN via miR-29. *Nat. Cell Biol.* **14**, 1322-1329.
Varelas, X. (2014). The Hippo pathway effectors TAZ and YAP in development, homeostasis and disease. *Development* **141**, 1614-1626.
Westerfield, M. (2007). *The Zebrafish Book: A guide for the laboratory use of zebrafish (Danio rerio)*. 4th edn. University of Oregon Press.
Yanagimachi, R., Cherr, G., Matsubara, T., Andoh, T., Harumi, T., Vines, C., Pillai, M., Griffin, F., Matsubara, H., Weatherby, T. et al. (2013). Sperm attractant in the micropyle region of fish and insect eggs. *Biol. Reprod.* **88**, 47.
Yang, C.-C., Graves, H. K., Moya, I. M., Tao, C., Hamaratoglu, F., Gladden, A. B. and Halder, G. (2015). Differential regulation of the Hippo pathway by adherens junctions and apical-basal cell polarity modules. *Proc. Natl. Acad. Sci. USA* **112**, 1785-1790.
Yimlamai, D., Christodoulou, C., Galli, G. G., Yanger, K., Pepe-Mooney, B., Gurung, B., Shrestha, K., Cahan, P., Stanger, B. Z. and Camargo, F. D. (2014). Hippo pathway activity influences liver cell fate. *Cell* **157**, 1324-1338.
Zhang, T., Zhou, Q. and Pignoni, F. (2011). Yki/YAP, Sd/TEAD and Hth/MEIS control tissue specification in the Drosophila eye disc epithelium. *PLoS ONE* **6**, e22278.
Zhao, B., Wei, X., Li, W., Udan, R. S., Yang, Q., Kim, J., Xie, J., Ikenoue, T., Yu, J., Li, L. et al. (2007). Inactivation of YAP oncoprotein by the Hippo pathway is involved in cell contact inhibition and tissue growth control. *Genes Dev.* **21**, 2747-2761.
Zhao, B., Ye, X., Yu, J., Li, L., Li, W., Li, S., Yu, J., Lin, J. D., Wang, C.-Y., Chinnaiyan, A. M. et al. (2008). TEAD mediates YAP-dependent gene induction and growth control. *Genes Dev.* **22**, 1962-1971.
Zhao, B., Tumaneng, K. and Guan, K.-L. L. (2011). The Hippo pathway in organ size control, tissue regeneration and stem cell self-renewal. *Nat. Cell Biol.* **13**, 877-883.